
Faculty of Engineering

Faculty Publications

A generalized model for dense axisymmetric grains flow with orientational diffusion

Amereh, M. & Nadler, B.

2022

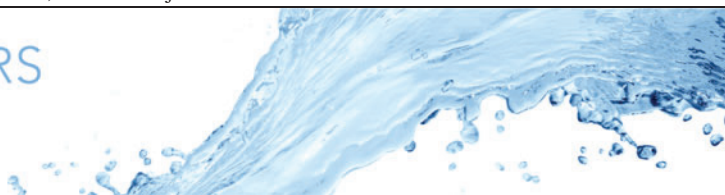
© 2022 Meitham Amereh et al. This is an open access article distributed under the terms of the Creative Commons Attribution License.

<http://creativecommons.org/licenses/by/4.0/>

This article was originally published at:
<https://doi.org/10.1017/jfm.2022.44>

Citation for this paper:

Amereh, M. & Nadler, B. (2022). "A generalized model for dense axisymmetric grains flow with orientational diffusion." *Journal of Fluid Mechanics*, 936, A40.
<https://doi.org/10.1017/jfm.2022.44>



A generalized model for dense axisymmetric grains flow with orientational diffusion

Meitham Amereh¹ and Ben Nadler^{1,†}

¹Department of Mechanical Engineering, University of Victoria, Victoria, BC V8W 2Y2, Canada

(Received 18 June 2021; revised 20 December 2021; accepted 29 December 2021)

The flow of non-spherical grains is strongly affected by the orientation of the grains, as observed in experiments and simulations. An existing model that predicts the orientation of grains as a function of the flow field and shape of the grains, is limited to homogenous orientational fields where the interaction of the grains with their surroundings is negligible. To address this limitation, we generalized the model to account for inhomogeneous orientational fields in the form of spatial non-convective orientational flux. The orientational flux accounts for the interactions of grains with their surroundings and the boundaries. The proposed model is used to study the influence of orientational diffusion and boundary conditions on the flow of dense granular material down an incline. It is shown that the boundary conditions can play a significant role in the orientation of grains in such flows.

Key words: dry granular material

1. Introduction

The study of granular flow in the liquid phase is an active research area with many open questions. Classical kinetic theory has shown successful predictions of granular flows with certain range of volume fraction (Garzó & Dufty 1999). However, alternative models such as non-local inertia rheology and other phenomenological models, have been used for dense granular flows (MiDi 2004; Jenkins & Berzi 2010; Gollin, Berzi & Bowman 2017). Our understanding of dense granular flow was advanced by important contributions (MiDi 2004; Campbell 2006; Jop, Forterre & Pouliquen 2006; Jiang & Liu 2009; Kamrin & Koval 2012; Zhang & Kamrin 2017), but it is mainly limited to spherical grains for which the orientation does not play a role. Although most of the naturally occurring granular media present a certain degree of asphericity (Cleary & Sawley 2002; González-Montellano, Ayuga & Ooi 2011; Matsushima & Chang 2011),

† Email address for correspondence: bnadler@uvic.ca

still, for the majority of research, granular flows are composed of spherical grains (Silbert *et al.* 2001; Delannay *et al.* 2007; Katsuragi, Abate & Durian 2010; Weinhart *et al.* 2012; Fall *et al.* 2015).

The rheology of axisymmetric grains was shown to have a complex response due to their tendency to align with respect to the flow and each other. It was observed that shear flows induce grains alignment which depends on the shape of the grains. The alignment was examined both experimentally, including photo-elastic particles (Tang & Behringer 2016), and numerically, using discrete element method (DEM) simulations in Wegner *et al.* (2012), Börzsönyi *et al.* (2012) and Hidalgo *et al.* (2018). To mathematically model the tendency of axisymmetric grains to align, a kinematic continuum model that captures the evolution of grains orientation subjected to homogenous flow was introduced in Nadler, Guillard & Einav (2018). In addition, the rheology of axisymmetric grains was investigated in Berzi *et al.* (2016, 2017), Trulsson (2018), Nath & Heussinger (2019), Nagy *et al.* (2017) and Nagy *et al.* (2020) using DEM, where it was shown that the rheological response has a strong dependency on the microstructure contacts and collisions which are primarily a function of the grains' orientation, alignment and shape. Based on these observations, an anisotropic rheology model (Nadler 2021) was proposed that accounts for the microstructure orientation. Typically, homogenous simple shear flows are used to investigate the response of non-spherical granular media, hence, we have fairly limited knowledge of the response to general inhomogeneous flows. The orientation and velocity fields of hopper flows were measured in Guillard, Marks & Einav (2017) using advanced X-ray radiography techniques. A steady-state flow of non-spherical grains down an incline was studied in Hidalgo *et al.* (2018) both experimentally and using DEM. This is a much simpler flow that is inhomogeneous and, as such, provides important observation that can enhance our understanding of more complex flows. This includes the role of interactions between the grains and their surroundings as well as the boundaries.

It is essential to obtain a realistic model which can predict the orientation and alignment of grains as they are identified as important factors in dense flow of non-spherical grains. The model proposed in Nadler *et al.* (2018) is able to well predict the orientation based on the grain's shape and the velocity field, however, it does not account for the interactions of grains with their surroundings and the boundaries. In this paper, we address this limitation by generalizing the model to include a non-convective spatial orientation flux. We also propose a jump boundary condition which incorporates the influence of the boundary flux to account for the interaction of grains with the boundaries. The performance of the proposed model and the influence of the model parameters are studied by simulating flows down an incline. It is shown that the generalized model can well capture the effect of inhomogeneous orientational fields.

The outline of the paper is as follows. Section 2 develops the proposed generalized orientation model and the associate boundary conditions. Section 3 presents the balance laws and the anisotropic inertia rheology model. Simulations of granular flows down an incline and the study of the model parameters are included in § 4. Finally, § 5 discusses the conclusions.

2. Orientation of axisymmetric grains

The ability of axisymmetric grains to orient and align introduces an additional degree of complexity to their mechanical response. Experimental and numerical measurements suggest that the orientation and alignment of these grains react to the flow and the boundary conditions. A convenient representation of the grains' orientation can be

constructed by taking the second moment of the orientation distribution

$$\mathbf{A} = \oint_{s^2} f(\mathbf{k}) \mathbf{k} \otimes \mathbf{k} \, da, \tag{2.1}$$

where $\pm \mathbf{k}$ is the orientation, $f(\mathbf{k}) \geq 0$ is the probability density function, s^2 denotes the unit sphere and $\oint_{s^2} f(\mathbf{k}) \, da = 1$. It follows from (2.1) that the orientational tensor \mathbf{A} is a second-order symmetric positive semi-definite tensor with a unit trace. It was proposed in Nadler *et al.* (2018) that the tendency of axisymmetric grains to align, when subjected to flow, can be well described by the evolution equation of the orientational tensor

$$\dot{\mathbf{A}} = \mathbf{W}\mathbf{A} - \mathbf{A}\mathbf{W} + \lambda [\mathbf{A}\mathbf{D} + \mathbf{D}\mathbf{A} - 2[\mathbf{D} \cdot \mathbf{A}]\mathbf{A}] - \psi D' [\mathbf{A} - \mathbf{I}/3], \tag{2.2}$$

where $\dot{\mathbf{A}}$ is the material time derivative of the orientational tensor, \mathbf{W} is the vorticity tensor, \mathbf{D} is the rate of deformation, \mathbf{I} is the identity tensor, $\mathbf{A} \cdot \mathbf{D} = \text{tr}(\mathbf{A}\mathbf{D}^T)$ is the tensor scalar product, λ and ψ are constitutive model parameters and $D' = \sqrt{\mathbf{D}' \cdot \mathbf{D}'}$ is the magnitude of the deviatoric part of the rate of deformation. Here we assume that the rate of collisions that drives the gains toward disorder is proportional to the magnitude of the deviatoric part of the rate of deformation. The phenomenological model parameters were determined by numerical simulations of simple shear flows using DEM (Nadler *et al.* 2018). It was assumed that the model parameters are only functions of the grain shape $r_g = (l - d)/(l + d)$, where l and d are the grain's geometrical length and diameter, respectively, and take the forms

$$\lambda(r_g) = (2/\pi) \tan^{-1}(5.5 r_g), \quad \psi(r_g) = 0.85 \exp(-4 r_g^2). \tag{2.3a,b}$$

As simple shear flow is primarily homogeneous, the role of orientational field could not be studied using these simulations and was not included in (2.2). In general, flow is not homogenous and, hence, orientational diffusion can play a significant role.

2.1. Orientational diffusion

The evolution law (2.2) was shown to perform well for homogeneous orientation and rate of deformation ($\text{grad } \mathbf{A} = \mathbf{0}$, $\text{grad } \mathbf{D} = \mathbf{0}$). In this case, the interaction through collisions and contacts with the surroundings was neglected. However, there are evidences that orientational diffusion is important (Guillard *et al.* 2017; Hidalgo *et al.* 2018). This is supported by Hidalgo *et al.* (2018) where flows down an incline were investigated and an inhomogeneous orientational field through the height was measured. We relate the inhomogeneous orientation field through the height of the flow to orientational diffusion. To include such orientational diffusion, the evolution equation (2.2) is generalized by adding a diffusion contribution. Recall that a general balance law has the form

$$\dot{\mathbf{A}} = \mathbf{P} + \text{div } \mathbf{G}, \tag{2.4}$$

where \mathbf{P} is a source term and \mathbf{G} is a non-convective flux term. In general, the source term includes supply and production, however, on physical ground, we eliminate the supply term and consider the source term to be only due to production. By comparison of (2.4) and (2.2), the right-hand side of (2.2) includes only the production term \mathbf{P} whereas the diffusion term $\text{div } \mathbf{G}$ is not included. Analogous to Fick's law for diffusion, we propose the non-convective flux \mathbf{G} to be proportional to the spatial gradient of the orientational tensor and the magnitude of the deviatoric part of the rate of deformation in the form

$$\mathbf{G} = \alpha D' \text{grad } \mathbf{A}, \tag{2.5}$$

where α is an orientational diffusion coefficient that has the dimensions of length squared. As diffusion occurs due to collisions, the diffusion flux is taken to be proportional to the

deviatoric part of the rate of deformation. The generalized evolution law takes the form

$$\dot{\mathbf{A}} = \mathbf{W}\mathbf{A} - \mathbf{A}\mathbf{W} + \lambda[\mathbf{A}\mathbf{D} + \mathbf{D}\mathbf{A} - 2[\mathbf{A} \cdot \mathbf{D}]\mathbf{A}] - \psi D' [\mathbf{A} - \mathbf{I}/3] + \text{div} [\alpha D' \text{grad } \mathbf{A}]. \tag{2.6}$$

This generalized evolution law (2.6) must satisfy two requirements that are studied in the following section.

2.2. Admissibility of the modified evolution law

The generalized evolution law is admissible if it guarantees that \mathbf{A} is positive semi-definite and it has a unit trace, $\text{tr } \mathbf{A} = 1$, for all processes. Utilizing the spectral representation of \mathbf{A} , these requirements can be verified by analyzing the evolution of the eigenvalues. The spectral representation of the symmetric orientational tensor \mathbf{A} has the form

$$\mathbf{A} = \sum_{i=1}^3 a_i \mathbf{a}_i \otimes \mathbf{a}_i, \tag{2.7}$$

where a_i are the eigenvalues and \mathbf{a}_i are the associated orthonormal eigenvectors. The Eigenvalues of the orientational tensor \mathbf{A} represent the portion of grains in the direction of the associated eigenvectors. The two requirements are satisfied if and only if all eigenvalues are non-negative, $a_i \geq 0$, and the summation of eigenvalues equals one, $a_1 + a_2 + a_3 = 1$. In the following sections, we prove that for all initial conditions that satisfy these two requirements, the generalized evolution law (2.6) guarantees that $\text{tr } \mathbf{A} = 1$ and all eigenvalues remain non-negative, for all processes. To show these, we utilize Cartesian coordinates $\{x_i\}$ and use the standard convenient notation $\square_{,i} = \partial \square / \partial x_i$ for partial derivatives. In the following derivations the summation convention does not apply. First, it is necessary to show that $\text{tr } \dot{\mathbf{A}} = 0$, which can be achieved by verifying that the evolution law (2.6) satisfies $\text{tr } \dot{\mathbf{A}} = 0$ for all processes.

PROPOSITION 2.1. *The evolution law satisfies $\text{tr } \dot{\mathbf{A}} = 0$ for all processes.*

Proof. It was already shown in Nadler *et al.* (2018) that the production term is traceless, that is

$$\text{tr} [\mathbf{W}\mathbf{A} - \mathbf{A}\mathbf{W} + \lambda(\mathbf{A}\mathbf{D} + \mathbf{D}\mathbf{A} - 2(\mathbf{D} \cdot \mathbf{A})\mathbf{A}) - \psi D'(\mathbf{A} - \mathbf{I}/3)] = 0. \tag{2.8}$$

Hence, it is only necessary to show that the diffusion term is traceless

$$\text{tr} [\text{div} [D' \alpha \text{grad}(\mathbf{A})]] = 0, \tag{2.9}$$

which can be expressed as

$$\sum_{j=1}^3 \left[(\alpha D')_{,j} \left(\sum_{i=1}^3 a_{i,j} \right) + \alpha D' \left(\sum_{i=1}^3 a_{i,jj} \right) \right] = 0, \tag{2.10}$$

where the detailed derivations are provided in the Appendix A. Recall that $\sum_{i=1}^3 a_i = 1$, hence by taking the spatial derivatives, the following identities hold

$$\sum_{i=1}^3 a_{i,j} = 0, \quad \sum_{i=1}^3 a_{i,jj} = 0. \tag{2.11a,b}$$

Substitutions of these identities into (2.10) yields

$$\text{tr} [\text{div} [\alpha D' \text{grad} (\mathbf{A})]] = 0, \tag{2.12}$$

which shows the desirable property

$$\text{tr} \dot{\mathbf{A}} = 0, \tag{2.13}$$

for all processes.

To show that the evolution law (2.6) does not yield negative eigenvalues, we consider the case when an eigenvalue vanishes. In this case, if the rate of evolution of that eigenvalue is non-negative, it cannot become negative. Given an admissible state, that is, all eigenvalues are non-negative, when an eigenvalue vanishes, $a_i = 0$, this is either a local minimum or it vanishes at some neighbourhood. For both cases we have the properties

$$a_i = 0, \quad a_{i,j} = 0, \quad a_{i,jj} \geq 0, \tag{2.14a-c}$$

for all j . It should be noted that (2.14a-c) are necessary conditions but not sufficient for a minimum. Next, it is necessary to show that if an eigenvalue vanishes, $a_i = 0$, the evolution law (2.6) guarantees that $\dot{a}_i \geq 0$ for all processes. ■

PROPOSITION 2.2. *The evolution law guarantees that all eigenvalues are non-negative for all processes.*

Proof. Consider the evolution of the orientational tensor defined in (2.2) and the spectral representation (2.7) where the eigenvectors form orthonormal basis such that $\mathbf{a}_i \cdot \mathbf{a}_j = \delta_{ij}$. The material time derivative of the orientational tensor is

$$\dot{\mathbf{A}} = \sum_{i=1}^3 \dot{a}_i \mathbf{a}_i \otimes \mathbf{a}_i + \sum_{i=1}^3 a_i \overline{\dot{\mathbf{a}}_i}. \tag{2.15}$$

Orthonormality of the eigenvectors can be expressed as $\dot{\mathbf{a}}_i \cdot \mathbf{a}_i = 0$ and $\mathbf{a}_{i,j} \cdot \mathbf{a}_i = 0$. Taking the scalar product of (2.15) with $\mathbf{a}_i \otimes \mathbf{a}_i$ yields expression for the time derivative of the eigenvalues as

$$\dot{a}_i = \dot{\mathbf{A}} \cdot \mathbf{a}_i \otimes \mathbf{a}_i. \tag{2.16}$$

Substitution of (2.6) and (2.14a-c) into (2.16) yields the instantaneous evolution law of the vanishing eigenvalue as

$$\dot{a}_i = \frac{1}{3} \psi D' + \alpha D' \sum_{j=1}^3 \left[a_{i,jj} + 2 \sum_{k=1}^3 a_k (\mathbf{a}_{k,j} \cdot \mathbf{a}_i)^2 \right], \tag{2.17}$$

where more details of the derivation are included in [Appendix A](#). As $D' > 0$, $\psi > 0$ and the term in the brackets is non-negative, then taking $\alpha > 0$ guarantees that $\dot{a}_i > 0$ when $a_i = 0$. This shows that given $\alpha > 0$, all the eigenvalues are non-negative for all processes. More specifically, because $\sum_{i=1}^3 a_i = 1$ and $a_i \geq 0$, then all the eigenvalues are bounded, i.e. $0 \leq a_i \leq 1$, as required. In general, the coefficient α can be function of all the invariants of \mathbf{D} , \mathbf{A} and $\text{grad} \mathbf{A}$ as well as the pressure, p , and the aspect ratio, r_g , and other properties of the grains. ■

2.3. Initial and boundary conditions

The evolution law in (2.6) is an initial boundary-valued problem, giving a first-order differential equation in time and a second-order differential equation in space. Therefore, proper initial and boundary conditions for \mathbf{A} are required. The initial value of \mathbf{A} in the domain must be specified as the initial conditions. In addition, the boundary conditions must be specified and can significantly change the orientational field and the associate flow. The boundary condition can be Dirichlet (imposing the value of \mathbf{A}), Neumann (imposing the value of the spatial derivative of \mathbf{A}) or mixed type. The interaction of the grains with the boundary is governed by the surface properties, grain orientation and the flow. Such interactions drive the grains to align with the boundary surface by providing orientational flux. Motivated by the orientational flux term proposed in (2.5) and the commonly used jump boundary condition, we introduce an orientational jump boundary condition, where we assert that the jump is proportional to the rate of collisions, that is, the deviatoric part of the rate of deformation, D' , and the gradient of \mathbf{A} in the normal direction to the boundary

$$[[\mathbf{A}]] = -\nu D' \frac{\partial \mathbf{A}}{\partial n}, \quad (2.18)$$

where $[[\mathbf{A}]] = \mathbf{A}^+ - \mathbf{A}_s$ is the jump, \mathbf{A}^+ is the orientation of grains in contact with the boundary, \mathbf{A}_s is the orientation of boundary surface, n is the normal direction to the boundary and ν is a scalar with dimensions of time \times length that characterizes the properties of the boundary interaction with the grains in contact. This jump boundary condition suggests that the orientational flux is proportional to the orientation jump, that is, the orientation of the grains in direct contact with the boundary depends on the flow and the properties of the boundary. The limit cases can be identified where $\nu \rightarrow 0$, yields no jump on the boundary, that is, the orientation of the grains in contact with the boundary is completely aligned with the boundary and $\nu \rightarrow \infty$, yields $\partial \mathbf{A} / \partial n = 0$, that is, the orientational flux from the boundary vanishes. On physical ground, $\nu \geq 0$ such that the orientational flux is in the same direction as the jump. In general, the coefficient ν can be a function of all the invariants of \mathbf{D} , \mathbf{A} and $\partial \mathbf{A} / \partial n$ as well as the pressure, p and the properties of the grains and the boundary surface.

The orientation evolution law (2.6) and the jump boundary conditions (2.18) complete the governing equations of the orientational tensor, given the vorticity, \mathbf{W} and the rate of deformation \mathbf{D} . Next, to close the set of governing equations, conservation of mass and the balance of linear momentum supplemented by a constitutive law are introduced, where the constitutive law is an explicit function of the orientational tensor and couples the response of the system.

3. Anisotropic $\mu(I)$ rheology of axisymmetric grains

The conservation of mass and balance of linear momentum are respectively used to solve for the density ρ and the velocity \mathbf{v} fields

$$\dot{\rho} + \rho \operatorname{div} \mathbf{v} = 0, \quad \rho \dot{\mathbf{v}} = \rho \mathbf{b} + \operatorname{div} \boldsymbol{\sigma}, \quad (3.1a,b)$$

where \mathbf{b} is the body force and $\boldsymbol{\sigma}$ is the Cauchy stress. The rheological response of granular media is described by a constitutive law for the stress $\boldsymbol{\sigma}$ developed in flowing grains. Physically, the rheological response is a macro-scale manifestation of the characteristic of the contacts and collisions between grains in the microstructure. The characteristic of the contacts and collisions strongly depends on the grains shape, roughness, orientation and flow which was investigated in Börzsönyi *et al.* (2012); Börzsönyi *et al.* (2016),

Guillard *et al.* (2017) and Nagy *et al.* (2017). It was observed (Nagy *et al.* 2017) that for simple shear flows, the required shear traction to maintain the flow, dramatically decreases as the grains become more aspherical. This response is contributed to the ability of axisymmetric grains to align with respect to the flow (Nadler 2021), which, in turn, yields a decrease in the resistance of grains to slip with respect to each other. Here, we adopted the simple form of anisotropic inertia rheology for incompressible flow, proposed in Nadler (2021) as

$$\boldsymbol{\sigma} = \tilde{\boldsymbol{\sigma}}(I, p, \mathbf{D}, \mathbf{A}; r_g) = -p\mathbf{I} + p\mu(I)\phi(r_g) \left[\bar{\mathbf{D}} + \eta(r_g) \left[\mathbf{A}\bar{\mathbf{D}} + \bar{\mathbf{D}}\mathbf{A} - 2/3 (\bar{\mathbf{D}} \cdot \mathbf{A}) \mathbf{I} \right] \right], \quad (3.2)$$

where $\bar{\mathbf{D}} = \mathbf{D}/D$ is the direction of the rate of deformation and $\mu(I)$ is the friction. The construction of (3.2) is a generalization of the isotropic inertia rheology (Jop, Forterre & Pouliquen 2006) which depends on the dimensionless inertia number $I = Dd/\sqrt{p/\rho_s}$, where $D = \sqrt{\mathbf{D} \cdot \mathbf{D}}$, d , p and ρ_s are the magnitude of the rate of deformation, grain diameter, pressure and the solid density, respectively. The phenomenological inertia rheology relation is $\mu(I) = \mu_s + \mu_1 I^\beta$, where μ_s , μ_1 and β are model parameters. The parameters ϕ and η are assumed to be only functions of the aspect ratio, r_g . The proposed inertia rheology is valid for incompressible flow, hence the conservation of mass is satisfied and the pressure is a Lagrange multiplier. For further discussion of the form (3.2) see Nadler (2021). The associate initial and boundary conditions of the velocity and stress fields are required for the solution of the conservation of mass and the balance of linear momentum. Two types of boundary conditions are considered which should be decomposed to the normal direction, \mathbf{n} , and the tangential direction to the boundary. In the normal direction, the boundary conditions have the form

$$[[\rho \mathbf{v}]] \cdot \mathbf{n} = 0 \quad \text{or} \quad \boldsymbol{\sigma} \mathbf{n} \cdot \mathbf{n} = -p_b, \quad (3.3)$$

which are the mass flux or the traction boundary conditions, respectively, and p_b is the prescribed pressure. In the tangential directions, the boundary conditions have the form

$$\mathbb{P}[[\mathbf{v}]] = -\mathbb{P}v_t \boldsymbol{\sigma} \mathbf{n} \quad \text{or} \quad \mathbb{P} \boldsymbol{\sigma} \mathbf{n} = \boldsymbol{\tau}_b, \quad (3.4)$$

where $\mathbb{P} = \mathbf{I} - \mathbf{n} \otimes \mathbf{n}$ is the projection, $[[\mathbf{v}]]$ is the velocity jump, v_t is a model parameter characterizing the interaction between the boundary surface and the flow and $\boldsymbol{\tau}_b$ is the prescribed tangential traction. The special case of the no-slip condition is $v_t = 0$, however, in general, the coefficient v_t can be a function of the invariants of \mathbf{v} and $\boldsymbol{\sigma}$ as well as the properties of the grains and the boundary surface.

4. Flow down an incline

The evolution law (2.6) can capture inhomogeneous orientational field for general flow, and can accommodate orientational boundary conditions. The standard experiment to study granular flows is a simple shear flow, however, such flow is primarily homogeneous which is too simple for our interest. Granular flow down an incline, depicted in figure 1, is relatively a simple flow that exhibits inhomogeneous fields. Flow down an incline was investigated experimentally and numerically in Hidalgo *et al.* (2018), where the orientational field was measured. We use the observations in Hidalgo *et al.* (2018) to examine the performance of the proposed model. However, the data provided in Hidalgo *et al.* (2018) does not include the orientation near the surface and, hence, cannot be compared with the prediction of the proposed model to understand the diffusion response and the orientational boundary conditions. For a steady flow, the inclination angle is

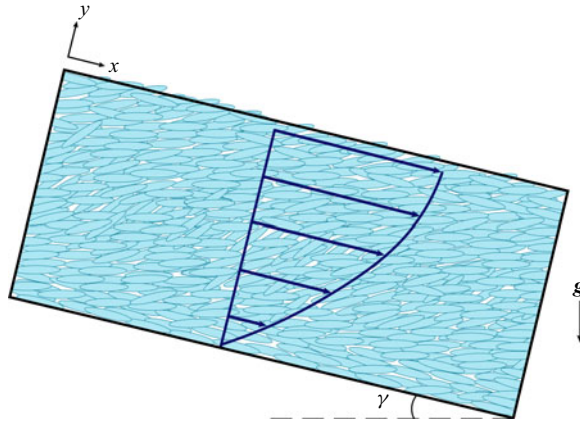


Figure 1. Schematic of flow of axisymmetric grains down an incline of angle γ .

bounded by a small angle below which no flow occurs, and a large angle above which no steady flow is possible because gravity overcomes the friction and acceleration persists. We investigate only an inclination angle where a steady-state flow exists. For our analysis, we consider a steady-state flow where the orientation, velocity and pressure are only functions of the height and are independent of time

$$p = p(y), \quad \mathbf{v} = v(y)\mathbf{i}, \quad \mathbf{A} = \mathbf{A}(y). \quad (4.1a-c)$$

It follows that at steady state

$$\dot{\mathbf{v}} = \frac{\partial \mathbf{v}}{\partial t} + (\text{grad } \mathbf{v}) \mathbf{v} = \mathbf{0}, \quad \dot{\mathbf{A}} = \frac{\partial \mathbf{A}}{\partial t} + (\text{grad } \mathbf{A}) \mathbf{v} = \mathbf{0}, \quad (4.2a,b)$$

and the governing equations are

$$\dot{\mathbf{A}} = \mathbf{0}, \quad \rho \mathbf{b} + \text{div } \boldsymbol{\sigma} = \mathbf{0}, \quad (4.3a,b)$$

where $\dot{\mathbf{A}}$ is defined in (2.6), the body force is $\mathbf{b} = g(\sin \theta \mathbf{i} + \cos \theta \mathbf{j})$ and $\boldsymbol{\sigma}$ has the form in (3.2). By (4.1a-c) and using the notation $v' = dv/dy$, the vorticity and the rate of deformation take the forms

$$\mathbf{W} = \frac{v'}{2} (\mathbf{i} \otimes \mathbf{j} - \mathbf{j} \otimes \mathbf{i}), \quad \mathbf{D} = \frac{v'}{2} (\mathbf{i} \otimes \mathbf{j} + \mathbf{j} \otimes \mathbf{i}). \quad (4.4a,b)$$

The boundary conditions (2.18), (3.3) and (3.4) are specified at the boundaries as

$$[[\mathbf{A}]] = v D' \frac{d\mathbf{A}}{dy}, \quad v = v_t \boldsymbol{\sigma} \mathbf{j} \cdot \mathbf{i}, \quad \text{at } y = 0, \quad (4.5)$$

$$\frac{d\mathbf{A}}{dy} = \mathbf{0}, \quad \boldsymbol{\sigma} \mathbf{j} = \mathbf{0}, \quad \text{at } y = h, \quad (4.6)$$

where (4.6)₁ imposes no orientational flux, and the free surface boundary condition is (4.6)₂. These provide a complete set of equations to solve for the unknown fields (4.1a-c). As this system of ordinary differential equations (ODEs) is nonlinear, numerical solutions are obtained using standard finite differences method. Convergence of the solution is verified by a sequence of grid refinements.

Here we are interested in studying the influence of the coefficients α and ν in the proposed generalized orientational model on the orientation, velocity and pressure fields.

Due to the lack of data, we do not attempt to relate the model coefficients directly to the grain's properties and the flow, but rather consider them as constants and investigate their influence on the model predictions. It should be noted that when α is taken to be a constant, then (2.6) becomes rate independent. Similar to Hidalgo *et al.* (2018), we consider the flow of cylindrical glass rods of diameter $d = 1.9$ mm and length $l = 3.5 d$ down an incline. The height of the steady state flow is set large enough compared to the size of grains, i.e. $H/d \approx 10^2$, such that a continuum model is valid. It follows that the aspect ratio is $r_g = 0.55$ and the value of the model parameters, $\lambda = 0.8$ and $\psi = 0.25$, are taken from Nadler *et al.* (2018). Although the evolution law of the orientation (2.6) is rate independent, the orientational boundary condition (2.18) is rate dependent for non-vanishing ν , hence, for $\nu > 0$, there is a coupling between the velocity and the orientational fields. In the following simulations, the values of the model parameters are

$$\begin{aligned} \phi = 1, \quad \eta = -0.9, \quad \rho_s = 2500 \text{ kg m}^{-3}, \quad \mu_s = 10^{-1}, \quad \mu_1 = 10^2, \quad \beta = 1, \\ \rho = 0.1 \text{ kg m}^{-3}, \quad \gamma = 30^\circ, \end{aligned} \tag{4.7a-h}$$

where the values of ϕ and η are taken from Nadler (2021), and for simplicity we adopt the no-slip condition, $v_t = 0$, for the velocity jump at the contact boundary. The properties of the particular grains including, shape (ellipsoidal, true cylinder), aspect ratio and internal friction are represented by the six model parameters.

To represent the orientational field, we define the preferred orientation as the angle of the largest eigenvalue with respect to the incline direction, calculated by

$$\theta = \tan^{-1} \frac{\mathbf{a}_3 \cdot \mathbf{j}}{\mathbf{a}_3 \cdot \mathbf{i}}, \tag{4.8}$$

where $0 \leq a_1 \leq a_2 \leq a_3 \leq 1$ are the sorted eigenvalues of \mathbf{A} , and $\{\mathbf{a}_1, \mathbf{a}_2, \mathbf{a}_3\}$ are the associated eigenvectors. For the measure of alignment, we consider the nematic order (Nagy *et al.* 2017) defined as the largest eigenvalue $1/3 \leq a_3 \leq 1$. Additional useful alignment measure is the ordering (Nadler *et al.* 2018; Nadler 2021) defined as

$$\zeta = \sqrt{\frac{1}{2} ((a_1 - a_2)^2 + (a_1 - a_3)^2 + (a_2 - a_3)^2)}, \tag{4.9}$$

where $0 \leq \zeta \leq 1$, such that, $\zeta = 0$ represents no alignment ($a_1 = a_2 = a_3 = 1/3$) and $\zeta = 1$ represents a full alignment ($a_1 = a_2 = 0, a_3 = 1$).

The following results are normalized with respect to the flow height

$$\bar{y} = \frac{y}{h}, \quad \bar{v} = \frac{v}{h}, \quad \bar{\alpha} = \frac{\alpha}{h^2}, \quad \bar{\nu} = \frac{\nu}{h}, \tag{4.10a-d}$$

and the inclined plane is considered to be perfectly flat in the xz plane, hence its orientation is described by

$$\mathbf{A}_s = \frac{1}{2} (\mathbf{i} \otimes \mathbf{i} + \mathbf{k} \otimes \mathbf{k}). \tag{4.11}$$

The boundary orientation, \mathbf{A}_s , represents the topology and orientation of the boundary surface, that is, for irregular boundary surface the boundary orientation should take a more isotropic form $\mathbf{A}_s \rightarrow I/3$.

Figures 2 and 3 show the influence of the diffusion coefficient, $\bar{\alpha}$, and the jump coefficient, $\bar{\nu}$, on the orientational field represented by the preferred orientation θ , the nematic order, a_3 , and the ordering ζ . These figures show results for $\bar{\alpha} = \{0.001, 0.005, 0.01\}$ and $\bar{\nu} = \{0, 0.02, 0.05\}$. Figure 2 depicts the influence of the diffusion coefficient and figure 3 depicts the influence of the orientational boundary jump.

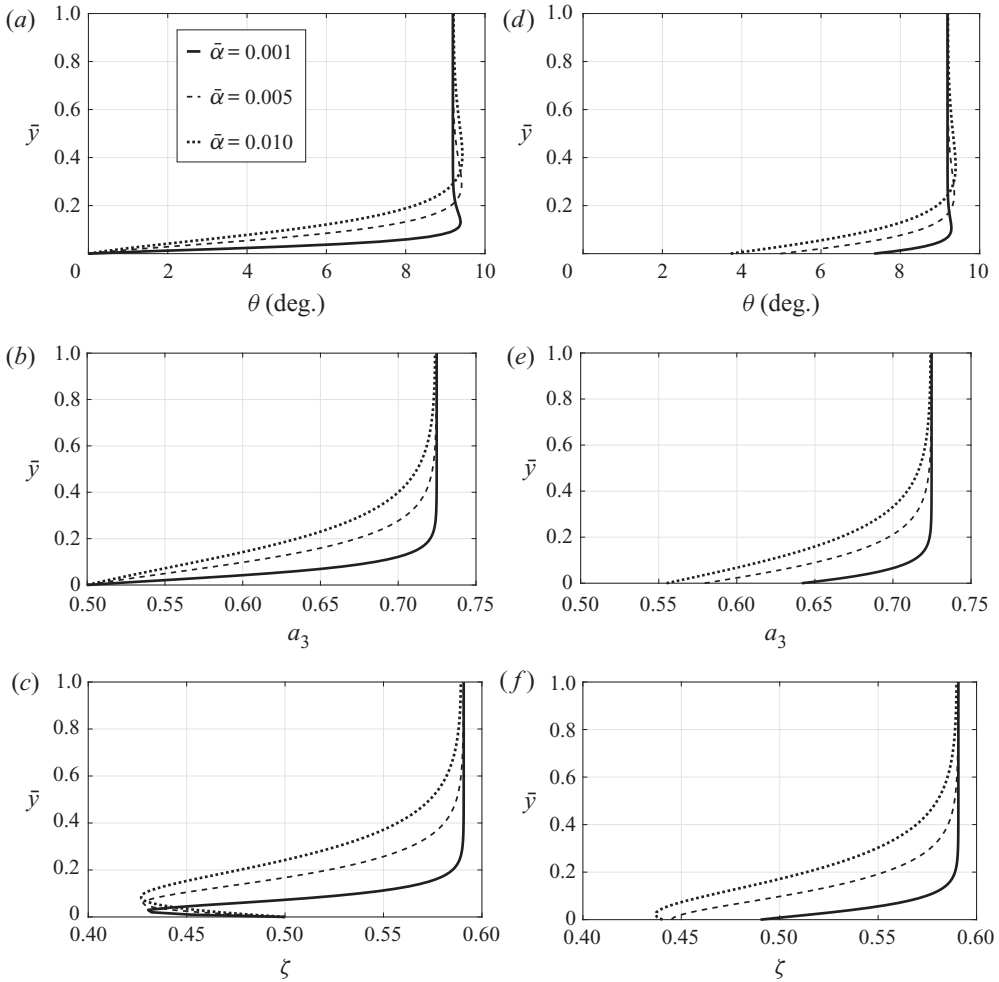


Figure 2. The influence of the diffusion coefficient, $\bar{\alpha}$, on the orientational angle, nematic order and ordering fields for $\bar{v} = 0$ and $\bar{v} = 0.05$: (a) $\bar{v} = 0$, (b) $\bar{v} = 0$, (c) $\bar{v} = 0$, (d) $\bar{v} = 0.05$, (e) $\bar{v} = 0.05$ and (f) $\bar{v} = 0.05$.

Larger values of the diffusion coefficient are not presented because the orientation does not reach an equilibrium state, and larger values of the orientational boundary jump are not presented because they eliminate the influence of the boundary. Figures 2(a,d) and 3(a,d) show, as expected, that a larger diffusion coefficient enhances the influence of the boundary, where the equilibrium orientation is obtained further away from the boundary. It is very interesting to note that the orientational angle θ shows a non-monotonic response, where the angle increases as the grains located at some distance from the boundary reach a maximum value and then decreases to the equilibrium angle far enough from the boundary as depicted in figure 2(a,d). This non-monotonic field, predicted by the model, is consistent with the orientational angle observed in Hidalgo *et al.* (2018). This non-monotonic field is due to the orientational flux from the boundary and, hence, reduces with a larger orientational boundary jump as depicted in figure 3(a,d). In these figures, for $\bar{v} = 0$ (no orientational boundary jump), the grains in contact with the boundary plane are completely aligned with the plane, but for larger \bar{v} , the orientation of grains in contact with the boundary plane approaches the equilibrium orientation yielding a more homogenous

Flow of axisymmetric grains with orientational diffusion

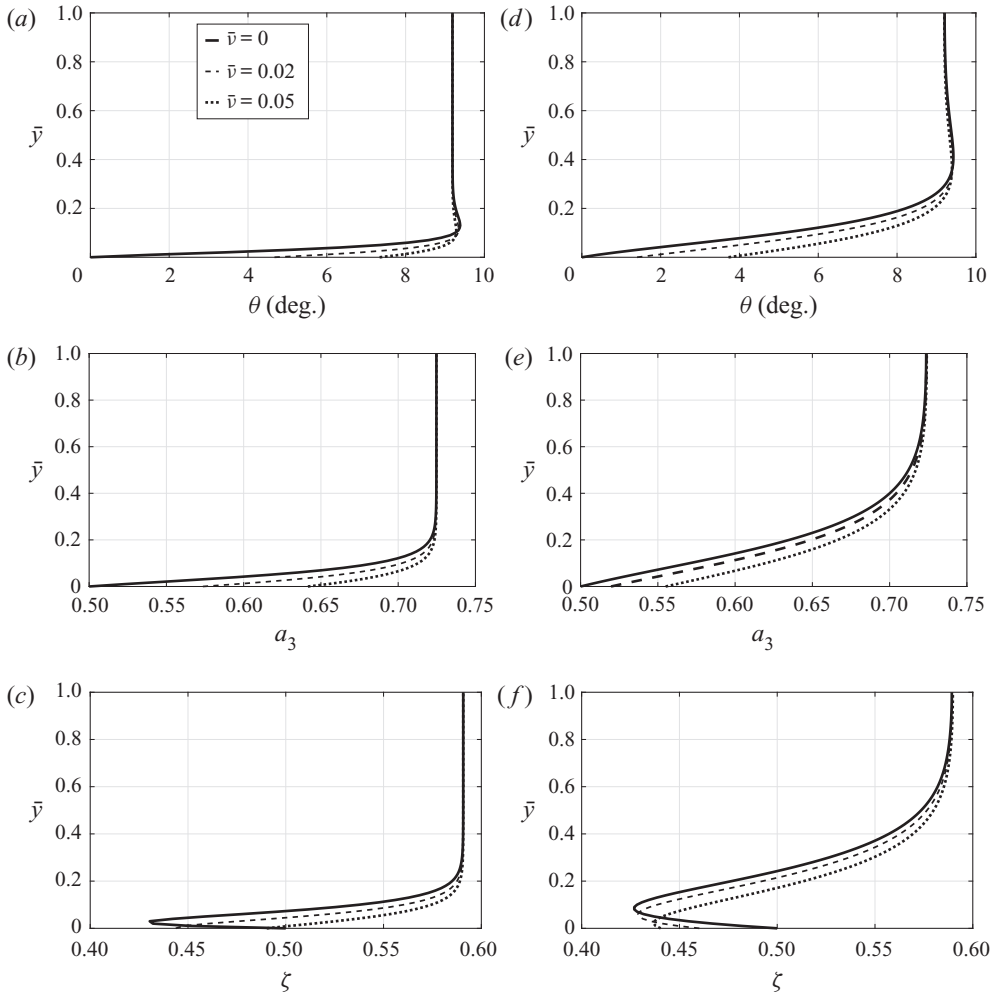


Figure 3. The influence of the jump coefficient, $\bar{\nu}$, on the orientational angle, nematic order and ordering fields for $\bar{\alpha} = 0.001$ and $\bar{\alpha} = 0.01$: (a) $\bar{\alpha} = 0.001$, (b) $\bar{\alpha} = 0.001$, (c) $\bar{\alpha} = 0.001$, (d) $\bar{\alpha} = 0.01$, (e) $\bar{\alpha} = 0.01$ and (f) $\bar{\alpha} = 0.01$.

orientational field. It is observed that the diffusion coefficient controls the location of the maximum angle, and the orientational boundary jump coefficient controls the magnitude of the maximum angle. Figures 2(b,e) and 3(b,e) show that the nematic order measured by the largest eigenvalue is minimum at the boundary and converges to the equilibrium away from the boundary, where the diffusion coefficient controls the rate of convergence. The equilibrium state is associated with vanishing orientational flux; hence, the orientation of the grains is governed only by the production term in (2.6) as was studied in Nadler *et al.* (2018) for homogeneous fields. As the orientational flux from the boundary reduces, for increasing values of $\bar{\nu}$, the nematic order becomes more homogeneous. Figures 2(c,f) and 3(c,f) show a non-monotonic field of the ordering ζ , which accounts for the overall alignment. For $\nu = 0$, the grains in contact with the boundary are forced by the no-jump orientational boundary condition to be in a state of isotropic distribution in the xz plane (transverse isotropy). As grains that are oriented in the $\mathbf{k} \otimes \mathbf{k}$ direction near the boundary rotate toward the equilibrium state away from the boundary, the overall ordering shows a

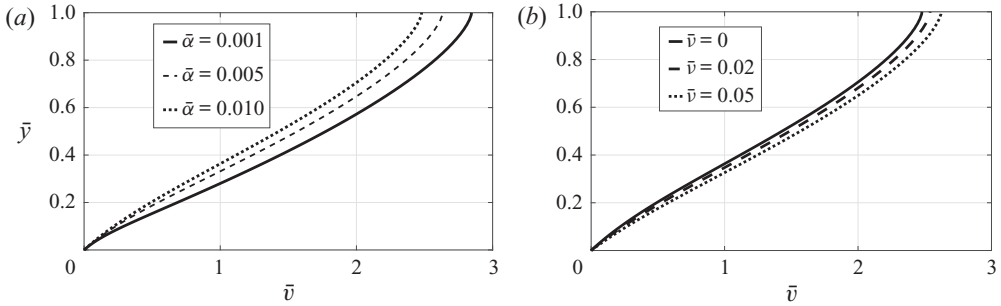


Figure 4. The influence of the diffusion coefficient, $\bar{\alpha}$, and orientational boundary jump coefficients, $\bar{\nu}$, on the velocity profile: (a) $\bar{\nu} = 0$ and (b) $\bar{\alpha} = 0.01$.

non-monotonic field with the minimum near the boundary where the diffusion coefficient governs the distance from the boundary. This non-monotonic response diminishes, as depicted in figures 2(c,f) and 3(c,f), for larger values of the boundary orientational jump $\bar{\nu}$ associated with decrease of the boundary flux the equilibrium state is obtained closer to the boundary. In addition, figures 2 and 3 demonstrate that the jump boundary condition (2.18) yields flow-dependent orientation of the grains in direct contact with the boundary. As can be observed in figures 2 and 3, the size of the boundary layer increases with the orientation diffusion coefficient as the boundary flux diffuses further into the bulk. Here we limit the values of the orientational diffusion, $\bar{\alpha}$, such that the equilibrium orientation is obtain within the domain. However, for larger values of the orientation diffusion the equilibrium orientation is not obtained within the domain.

It is demonstrated that the generalized model can well capture an inhomogeneous orientational field and accounts for the boundary condition. The response is complex with non-monotonic orientational field which is enhanced by the influence of the boundaries. The orientational diffusion coefficient models the microstructure interaction between grains that drives the grains to align with respect to the surroundings, and is expected to increase as the grains become more aspherical. In addition, the boundary affects the orientational field by means of orientational flux from the boundary. This boundary flux accounts for the interaction between the boundary and the grains, which is characterized by the orientation of the boundary, \mathbf{A}_s , and the orientational boundary jump coefficient.

The rheological model (3.2) has an explicit dependency on the orientation, therefore, the velocity profile depends on the orientational field. Figure 4 depicts the velocity profiles for various diffusion coefficients and orientational boundary jump coefficients. In figure 4(a), it is shown that the velocity decreases as the diffusion coefficient increases, which is directly related to the rheological property that the flow resistance decreases as grains become more aligned with the flow. With increasing orientational diffusion the grains are more affected by the orientational boundary flux and, hence, less aligned. Similarly, as the orientational boundary jump coefficient increases, the orientational boundary flux decreases, yielding a higher grains alignment that induces lower flow resistance, hence higher velocity, as depicted in figure 4(b). At steady state, the balance of linear momentum (3.1a,b)₂ takes the form

$$\frac{d\sigma_{12}}{dy} = -\rho g \sin \gamma, \quad \frac{d\sigma_{22}}{dy} = -\rho g \cos \gamma, \quad (4.12a,b)$$

Flow of axisymmetric grains with orientational diffusion

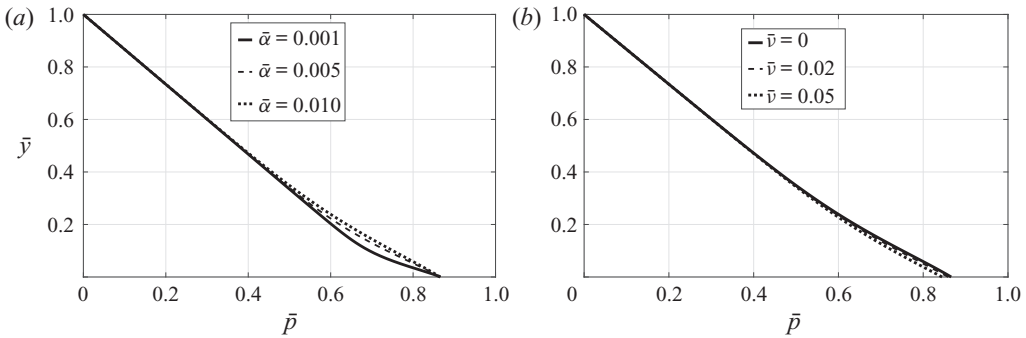


Figure 5. The influence of the diffusion coefficient, $\bar{\alpha}$, and boundary jump coefficients, $\bar{\nu}$, on the pressure profile: (a) $\bar{\nu} = 0$ and (b) $\bar{\alpha} = 0.01$.

hence, σ_{12} and σ_{22} are linear in height together with the boundary conditions (4.6) and (4.7a–h) take the forms

$$\sigma_{12} = (\bar{y} - 1)h\rho g \sin \gamma, \quad \sigma_{22} = (\bar{y} - 1)h\rho g \cos \gamma. \quad (4.13a,b)$$

It should be noted that due to the anisotropy of the rheological model (3.2), the orientation and flow contribute to the normal stress in addition to the pressure. Hence, although the normal stress, σ_{22} , is linear, the pressure field is not. Figure 5 depicts the normalized pressure $\bar{p} = p/(\rho gh)$, where it can be seen in figure 5(a) that the pressure deviation from linear profile increases as the diffusion coefficient decreases and the orientational field becomes more inhomogeneous. Similarly, as the boundary jump coefficients increases the pressure deviation from linear profile decreases due to the decrease in orientational boundary flux, which yields a more homogenous orientational field, as depicted in figure 5(b).

5. Conclusion

In this paper, we have generalized a previously developed kinematic model for the orientation of axisymmetric grains by including orientational diffusion that accounts for the interactions of grains with their surroundings. This has been obtained by introducing a new non-convective orientational flux term, inspired by the classical transport approach. The flux is taken to be proportional to the orientation gradient, the magnitude of the deviatoric part of the rate of deformation, and is characterized by a single diffusion coefficient. In the present model granular temperature is not included explicitly, however, in a more complete theory that includes velocity fluctuations, the orientational flux should be driven by the granular temperature.

It has been proved mathematically that the proposed model complies with all the properties of the orientational tensor. An orientational jump condition is also introduced to model the interaction with the boundary. To investigate the performance of the model, flows down an incline are studied. We have adopted an anisotropic inertia rheology as a constitutive law for the stresses. It has been shown that the proposed model is simple, but capable of predicting the complex behaviour of the orientation of axisymmetric grains subjected to inhomogeneous flows. Comparison with experiments on flows down an incline has shown that the model provides a realistic description of the orientational field. However, more experimental data of the grains orientation near the boundary surface is required to further evaluate the accuracy of the model.

The influence of the granular properties, such as grains shape and internal friction, on the orientational diffusion is an open questions that we do not have supporting data to answer. However, from a consideration of the microstructure contacts and collisions between grains, we anticipate that the diffusion coefficient increases as the axisymmetric grains become more aspherical. The influence of the internal friction on the orientational diffusion is even more complex to envision. To answer these important questions we need more experimental data and DEM simulations to understand the influence of shape and friction on the orientational diffusion.

Acknowledgements. All authors were involved in all aspects of the manuscript including model development, simulations and writing the manuscript.

Funding. We wish to confirm that there has been no significant financial support for this work that could have influenced its outcome.

Declaration of interests. The authors report no conflict of interest.

Author ORCIDs.

Meitham Amereh <https://orcid.org/0000-0002-5035-9244>;

Ben Nadler <https://orcid.org/0000-0001-7299-5842>.

Appendix A

Establishing the following identities are useful to prove propositions 2.1 and 2.2. The terms in the modified evolution law (2.6) can be expressed using the spectral representation of the orientational tensor and the associate evolution of the eigenvalues (2.16). Using the skew-symmetry of the vorticity tensor, \mathbf{W} , the following identities can be established

$$\mathbf{W}\mathbf{A} \cdot \mathbf{a}_i \otimes \mathbf{a}_i = \left(\sum_{j=1}^3 a_j \mathbf{W}\mathbf{a}_j \otimes \mathbf{a}_j \right) \cdot \mathbf{a}_i \otimes \mathbf{a}_i = a_i (\mathbf{W}\mathbf{a}_i \cdot \mathbf{a}_i) = 0, \quad (\text{A1})$$

and similarly $\mathbf{A}\mathbf{W} \cdot \mathbf{a}_i \otimes \mathbf{a}_i = 0$. The symmetry of the rate of deformation, \mathbf{D} , yields

$$\mathbf{A}\mathbf{D} \cdot \mathbf{a}_i \otimes \mathbf{a}_i = \left(\sum_{j=1}^3 a_j \mathbf{a}_j \otimes \mathbf{D}\mathbf{a}_j \right) \cdot \mathbf{a}_i \otimes \mathbf{a}_i = a_i (\mathbf{D}\mathbf{a}_i \cdot \mathbf{a}_i) = a_i D_{ii}, \quad (\text{A2})$$

and similarly $\mathbf{D}\mathbf{A} \cdot \mathbf{a}_i \otimes \mathbf{a}_i = a_i D_{ii}$. Direct results are $(\mathbf{A} \cdot \mathbf{D})\mathbf{A} \cdot \mathbf{a}_i \otimes \mathbf{a}_i = a_i (\mathbf{A} \cdot \mathbf{D})$ and $\psi D'(\mathbf{A} - \mathbf{I}/3) \cdot \mathbf{a}_i \otimes \mathbf{a}_i = \psi D'(a_i - 1/3)$. Finally,

$$\begin{aligned} \text{div}[\alpha D' \text{grad}(\mathbf{A})] &= \sum_{j=1}^3 \sum_{i=1}^3 [(\alpha D')_{,j} (a_{i,j} \mathbf{a}_i \otimes \mathbf{a}_i + a_i (\mathbf{a}_{i,j} \otimes \mathbf{a}_i + \mathbf{a}_i \otimes \mathbf{a}_{i,j})) \\ &\quad + \alpha D' (a_{i,jj} \mathbf{a}_i \otimes \mathbf{a}_i + 2a_{i,j} (\mathbf{a}_{i,j} \otimes \mathbf{a}_i + \mathbf{a}_i \otimes \mathbf{a}_{i,j}) \\ &\quad + a_i (\mathbf{a}_{i,jj} \otimes \mathbf{a}_i + 2\mathbf{a}_{i,j} \otimes \mathbf{a}_{i,j} + \mathbf{a}_i \otimes \mathbf{a}_{i,jj}))]. \end{aligned} \quad (\text{A3})$$

The following identities can be established using $\mathbf{a}_i \cdot \mathbf{a}_j = \delta_{ij}$ by taking spatial derivatives

$$\mathbf{a}_{i,m} \cdot \mathbf{a}_j + \mathbf{a}_i \cdot \mathbf{a}_{j,m} = 0, \quad \mathbf{a}_{i,mm} \cdot \mathbf{a}_j + \mathbf{a}_{i,m} \cdot \mathbf{a}_{j,n} + \mathbf{a}_{i,n} \cdot \mathbf{a}_{j,m} + \mathbf{a}_i \cdot \mathbf{a}_{j,mm} = 0 \quad (\text{A4a,b})$$

for all i, j, m and n . Taking $j = i$ and $n = m$ yields the useful identities $\mathbf{a}_{i,m} \cdot \mathbf{a}_i = 0$ and $\mathbf{a}_{i,mm} \cdot \mathbf{a}_i + \mathbf{a}_{i,m} \cdot \mathbf{a}_{i,m} = 0$. Substituting (A3) and (A4) into (2.16) yields

$$\text{tr} [\text{div} [D' \alpha \text{grad}(\mathbf{A})]] = \sum_{j=1}^3 \left[(\alpha D')_{,j} \left(\sum_{i=1}^3 a_{i,j} \right) + \alpha D' \left(\sum_{i=1}^3 a_{i,jj} \right) \right], \quad (\text{A5})$$

$$\begin{aligned} & \operatorname{div} [D' \alpha \operatorname{grad} (\mathbf{A})] \cdot \mathbf{a}_i \otimes \mathbf{a}_i \\ &= \sum_{j=1}^3 \left[(\alpha D')_{,j} a_{i,j} + \alpha D' \left(a_{i,jj} + 2a_i(\mathbf{a}_{i,jj} \cdot \mathbf{a}_i) + 2 \sum_{k=1}^3 a_k (\mathbf{a}_{k,j} \cdot \mathbf{a}_i)^2 \right) \right]. \end{aligned} \quad (\text{A6})$$

Substituting (A1), (A2), (A3), (A6) and (2.6) into (2.16) yields

$$\begin{aligned} \dot{a}_i &= 2\lambda (D_{ii} - (\mathbf{A} \cdot \mathbf{D})) a_i + \psi D' (1/3 - a_i) \\ &+ \sum_{j=1}^3 \left[(\alpha D')_{,j} a_{i,j} + \alpha D' \left(a_{i,jj} + 2a_i(\mathbf{a}_{i,jj} \cdot \mathbf{a}_i) + 2 \sum_{k=1}^3 a_k (\mathbf{a}_{k,j} \cdot \mathbf{a}_i)^2 \right) \right]. \end{aligned} \quad (\text{A7})$$

REFERENCES

- BERZI, D., THAI-QUANG, N., GUO, Y. & CURTIS, J. 2016 Stresses and orientational order in shearing flows of granular liquid crystals. *Phys. Rev. E* **93**, 040901.
- BERZI, D., THAI-QUANG, N., GUO, Y. & CURTIS, J. 2017 Collisional dissipation rate in shearing flows of granular liquid crystals. *Phys. Rev. E* **95**, 050901.
- BÖRZSÖNYI, T., SOMFAI, E., SZABÓ, B., WEGNER, S., MIER, P., ROSE, G. & STANNARIUS, R. 2016 Packing, alignment and flow of shape-anisotropic grains in a 3D silo experiment. *New J. Phys.* **18** (9), 093017.
- BÖRZSÖNYI, T., SZABÓ, B., TÖRÖS, G., WEGNER, S., TÖRÖK, J., SOMFAI, E., BIEN, T. & STANNARIUS, R. 2012 Orientational order and alignment of elongated particles induced by shear. *Phys. Rev. Lett.* **108** (22), 228302.
- CAMPBELL, C.S. 2006 Granular material flows—an overview. *Powder Technol.* **162** (3), 208–229.
- CLEARY, P.W. & SAWLEY, M.L. 2002 DEM modelling of industrial granular flows: 3D case studies and the effect of particle shape on hopper discharge. *Appl. Math. Model.* **26** (2), 89–111.
- DELANNAY, R., LOUGE, M., RICHARD, P., TABERLET, N. & VALANCE, A. 2007 Towards a theoretical picture of dense granular flows down inclines. *Nat. Mater.* **6** (2), 99–108.
- FALL, A., OVARLEZ, G., HAUTEMAYOU, D., MÉZIERE, C., ROUX, J.-N. & CHEVOIR, F. 2015 Dry granular flows: rheological measurements of the μ (i)-rheology. *J. Rheol.* **59** (4), 1065–1080.
- GARZÓ, V. & DUFTY, J. 1999 Dense fluid transport for inelastic hard spheres. *Phys. Rev. E* **59** (5), 5895.
- GOLLIN, D., BERZI, D. & BOWMAN, E.T. 2017 Extended kinetic theory applied to inclined granular flows: role of boundaries. *Granul. Matt.* **19** (3), 56.
- GONZÁLEZ-MONTELLANO, C., AYUGA, F. & OOI, J. 2011 Discrete element modelling of grain flow in a planar silo: influence of simulation parameters. *Granul. Matt.* **13** (2), 149–158.
- GUILLARD, F., MARKS, B. & EINAIV, I. 2017 Dynamic x-ray radiography reveals particle size and shape orientation fields during granular flow. *Sci. Rep.* **7** (1), 8155.
- HIDALGO, R.C., SZABÓ, B., GILLEAROT, K., BÖRZSÖNYI, T. & WEINHART, T. 2018 Rheological response of nonspherical granular flows down an incline. *Phys. Rev. Fluids* **3**, 074301.
- JENKINS, J.T. & BERZI, D. 2010 Dense inclined flows of inelastic spheres: tests of an extension of kinetic theory. *Granul. Matt.* **12** (2), 151–158.
- JIANG, Y. & LIU, M. 2009 Granular solid hydrodynamics. *Granul. Matt.* **11** (3), 139.
- JOP, P., FORTERRE, Y. & POULIQUEN, O. 2006 A constitutive law for dense granular flows. *Nature* **441** (7094), 727–730.
- KAMRIN, K. & KOVAL, G. 2012 Nonlocal constitutive relation for steady granular flow. *Phys. Rev. Lett.* **108** (17), 178301.
- KATSURAGI, H., ABATE, A. & DURIAN, D. 2010 Jamming and growth of dynamical heterogeneities versus depth for granular heap flow. *Soft Matt.* **6** (13), 3023–3029.
- MATSUSHIMA, T. & CHANG, C.S. 2011 Quantitative evaluation of the effect of irregularly shaped particles in sheared granular assemblies. *Granul. Matt.* **13** (3), 269–276.
- MIDI, G. 2004 On dense granular flows. *Eur. Phys. J. E* **14** (4), 341–365.
- NADLER, B. 2021 Anisotropic inertia rheology of ellipsoidal grains. *Granul. Matt.* **23** (1), 14.
- NADLER, B., GUILLARD, F. & EINAIV, I. 2018 Kinematic model of transient shape-induced anisotropy in dense granular flow. *Phys. Rev. Lett.* **120**, 198003.
- NAGY, D.B., CLAUDIN, P., BÖRZSÖNYI, T. & SOMFAI, E. 2017 Rheology of dense granular flows for elongated particles. *Phys. Rev. E* **96**, 062903.

- NAGY, D.B., CLAUDIN, P., BÖRZSÖNYI, T. & SOMFAI, E. 2020 Flow and rheology of frictional elongated grains. *New J. Phys.* **22** (7), 073008.
- NATH, T. & HEUSSINGER, C. 2019 Rheology in dense assemblies of spherocylinders: frictional vs. frictionless. *Eur. Phys. J. E* **42** (12), 157.
- SILBERT, L.E., ERTAŞ, D., GREY, G.S., HALSEY, T.C., LEVINE, D. & PLIMPTON, S.J. 2001 Granular flow down an inclined plane: Bagnold scaling and rheology. *Phys. Rev. E* **64** (5), 051302.
- TANG, J. & BEHRINGER, R.P. 2016 Orientation, flow, and clogging in a two-dimensional hopper: ellipses vs. disks. *Europhys. Lett.* **114** (3), 34002.
- TRULSSON, M. 2018 Rheology and shear jamming of frictional ellipses. *J. Fluid Mech.* **849**, 718–740.
- WEGNER, S., BÖRZSÖNYI, T., BIEN, T., ROSE, G. & STANNARIUS, R. 2012 Alignment and dynamics of elongated cylinders under shear. *Soft Matt.* **8**, 10950–10958.
- WEINHART, T., THORNTON, A.R., LUDING, S. & BOKHOVE, O. 2012 Closure relations for shallow granular flows from particle simulations. *Granul. Matt.* **14** (4), 531–552.
- ZHANG, Q. & KAMRIN, K. 2017 Microscopic description of the granular fluidity field in nonlocal flow modeling. *Phys. Rev. Lett.* **118** (5), 058001.